arXiv:cond-mat/0611694v1 [cond-mat.stat-mech] 28 Nov 2006

Slow relaxation in the two dimensional electron plasma under the strong magnetic field

Ryo KAWAHARA* and Hiizu NAKANISHI†

Department of Physics, Kyushu University 33, Fukuoka 812-8581.

(Received February 6, 2008)

We study slow relaxation processes in the point vortex model for the two-dimensional pure electron plasma under the strong magnetic field. By numerical simulations, it is shown that, from an initial state, the system undergoes the fast relaxation to a quasi-stationary state, and then goes through the slow relaxation to reach a final state. From analysis of simulation data, we find (i) the time scale of the slow relaxation increases linearly to the number of electrons if it is measured by the unit of the bulk rotation time, (ii) during the slow relaxation process, each electron undergoes an superdiffusive motion, and (iii) the superdiffusive motion can be regarded as the Levy flight, whose step size distribution is of the power law. The time scale that each electron diffuses over the system size turns out to be much shorter than that of the slow relaxation, which suggests that the correlation among the superdiffusive trajectories is important in the slow relaxation process.

KEYWORDS: non-neutral plasma, two-dimensional turbulence, numerical simulation, long range force, non-extensive system, slow relaxation, anomalous diffusion, Levy flight

1. Introduction

The system of pure electron plasma under the strong magnetic field has been of scientific interest for various aspects; Such a system does not satisfy the basic premise of the Boltzmann statistics, i.e. the existence of a subsystem weakly coupled to the rest, because the interaction between the constituent particles is long-range, consequently any part of the system interacts strongly with the rest. Under a certain experimentally realizable condition, the system behaves like a two-dimensional (2-d) system and is shown to be described as a 2-d point vortex system with a unit vorticity, whose continuum description reduces to the 2-d Euler equation of the incompressible inviscid fluid.[1]

Historically, the point vortex system is the system for which Onsager developed the idea of negative temperature in his statistical theory and predicted the equilibrium states of the large vortex cluster in the relaxation of 2-d high Reynolds number fluid.[2,3] His theory has been advanced,[4–6] and has been examined by simulations of several hundred particles (or vortices) to show that the equilibrium state is the vortex cluster that maximizes the one-body entropy.[7]

In contrast with these results, in recent 2-d electron plasma experiments, the system has been demonstrated to relax into several kinds of "stationary" or "metaequilibrium" states, including the minimum enstrophy state[8] and the vortex crystal state.[9] These are quite different from the above equilibrium state. There have been applied several statistical theories to understand these relaxed states, which includes the minimum enstrophy theory,[8] the fluid entropy theory,[10–12] the Tsallis statistics,[13] the regional entropy theory for the vortex crystal,[14] etc., but none of these theories have successfully described these states on a general ground.[15–18]

These two contradicting results suggest that the system is trapped in some states before reaching the equilibrium in the experiments. In fact, we show in the present work that these stationary states are only quasi-stationary and relaxes into the equilibrium state very slowly. This process of slow relaxation is the major subject of the present paper.

Actually, for the stellar system with gravitation, which is another example with long-range interaction, it has been known that there are two types of relaxation: the violent relaxation and the collisional relaxation. The violent relaxation[19,20] is the fast process which is caused by the complex mixing due to the macroscopic collective interaction. The dynamics is described by the Vlasov equation and the two-body "collisions" do not play any role. In contrast, the collisional relaxation[20,21] is the slow process caused by the collisions of the individual particles and the relaxation time scale is much longer than that of the violent relaxation. Such a relaxation has already been found and analyzed in the molecular dynamics simulations of self-gravitating system.[22,23] The separation of these two relaxations is considered to be peculiar to the systems with long-range interaction.

In the present system of the 2-d electron plasma under the strong magnetic field, there are also a fast and a slow relaxation. The fast relaxation from an initial state takes place through the violent motion of the stretching and folding in the density field due to the macroscopic collective motion, and leads the system to a quasi-stationary state. The dynamics is described by the 2-d Euler equation and the individual two-body collisions do not play any role. The typical time scale for this fast relaxation is the rotation time of the bulk of the system $\tau_{\rm rot}$.

In contrast, the relaxation after the quasi-stationary states towards the equilibrium is much slower than the fast relaxation.

Chavanis has presented a theoretical analysis on the

*E-mail : ryokawa@stat.phys.kyushu-u.ac.jp
†E-mail : naka4scp@mbox.nc.kyushu-u.ac.jp

dynamics of this system[24,25] using the analogous idea developed in the self-gravitating system. He predicted that the ratio of the slow relaxation time to the fast relaxation scales with the total number of particles N as $N/\ln N$, based on the idea that the relaxation takes place through the diffusion of the individual particles caused by collisions, which can be ignored in the violent relaxation.

For the *neutral* plasma under the strong magnetic field, the theoretical analysis by Taylor and McNamara[26] has shown that the individual particle motion converges to the normal diffusive behavior only slowly, and the limiting value of the diffusion coefficient have been found to depend on the system size, which implies anomalous diffusion is taking place. Dawson et al. have pointed out that such behavior of diffusion is attributed to occasional long jumps of the particles convected by large vortices.[27]

In some experiments of the 2-d fluid with vortices, the diffusion of tracer particles have been often found to be anomalous,[28,29] and a Levy flight analysis has been proposed.[30]

In this paper, we present the results of the numerical simulations on the point vortex system. We observe the N-dependence of the fast and slow relaxation times and find that they are consistent with those estimated by Chavanis. Special attention is on the diffusion process during the slow relaxation, for which we find an anomalous diffusion and analyze it in terms of the Levy flight.

The paper is organized as follows: In §2, we introduce the 2-d electron plasma system under a magnetic field and define the model. In §3, we briefly review some statistical theories. The simulation method is explained in §4 and results are described in comparison with the statistical theories in §5. We analyze these results in terms of the Levy flight in §6, and the summary and discussion are given in §7.

2. Model system and its behavior

2.1 Equations of motion

The physical system we consider is the pure electron plasma in a cylindrical container with the strong magnetic field $\boldsymbol{B}$ applied along the axis (Fig. 1). In a certain situation,[8,9] it has been shown that the interaction between the electrons can be approximated by the two-dimensional Coulomb force and the drift velocity $\boldsymbol{v}_i$ of the i-th electron in the plane perpendicular to $\boldsymbol{B}$ is given by

$$\boldsymbol{v}_i = \frac{\boldsymbol{E}(\boldsymbol{r}_i)\times\boldsymbol{B}}{B^2}, \tag{1}$$

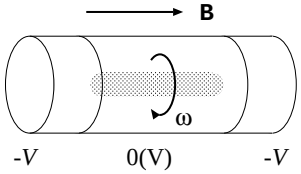

Fig. 1. Schematic diagram of Malmberg trap of the pure electron plasma.

disregarding the cyclotron motion. Here $\boldsymbol{E}(\boldsymbol{r})$ is the electric field and $\boldsymbol{r}_i$ is the position of i-th electron in the plane. Thus the electrons do not repel each other and can be contained in the cylinder (Malmberg Trap).

After some normalization, it can be shown[15] that the equations of motion for the electron position $\boldsymbol{r}_i = (x_i, y_i)$ are given by

$$\frac{dx_i}{dt} = \frac{\partial H}{\partial y_i}, \quad \frac{dy_i}{dt} = -\frac{\partial H}{\partial x_i}, \tag{2}$$

with the Hamiltonian H,

$$\begin{aligned} H &= -\frac{1}{2}\sum_i^N\sum_{j\neq i}^N G(\boldsymbol{r}_i,\boldsymbol{r}_j) - \frac{1}{2}\sum_i^N G_{\rm m}(\boldsymbol{r}_i,\boldsymbol{r}_i) \\ &= -\frac{1}{2}\sum_i^N \phi_i(\boldsymbol{r}_i), \end{aligned} \tag{3}$$

where $G(\boldsymbol{r}_i,\boldsymbol{r}_j)$ is the 2-d Green function for the electric potential that satisfies $\nabla^2 G(\boldsymbol{r},\boldsymbol{r}') = \delta(\boldsymbol{r}-\boldsymbol{r}')$ with an appropriate boundary condition, $G_{\rm m}(\boldsymbol{r},\boldsymbol{r}')$ is the electric potential at $\boldsymbol{r}$ brought about by the mirror charge induced by the charge at $\boldsymbol{r}'$, and $\phi_i(\boldsymbol{r})$ is the electric potential due to all the electrons except for the ith one. In the present case, we consider the system which is in a cylindrical container with the radius R_w, then ϕ_i is given by[31,32]

$$\begin{aligned} \phi_i(\boldsymbol{r}) \equiv &+ \frac{1}{2\pi}\sum_{j\neq i}^N \ln|\boldsymbol{z}-\boldsymbol{z}_j| \\ &- \frac{1}{2\pi}\sum_j^N\left[\ln|z-\frac{R_w^2}{z_j^*}| + \ln\frac{|z_j|}{R_w}\right], \end{aligned} \tag{4}$$

where $z = x+iy$ and z^* is the complex conjugate of z; the second term corresponds to the potential by the mirror charges.

2.2 Euler equation

Note that the density field

$$n(\boldsymbol{r}) = \sum_i \delta(\boldsymbol{r}-\boldsymbol{r}_i(t)) \tag{5}$$

with $\boldsymbol{r}_i(t)$ being a solution of eq. (2) gives a singular solution for the set of equations,

$$\frac{Dn}{Dt} \equiv \frac{\partial n}{\partial t} + \boldsymbol{v}\cdot\nabla n = 0, \tag{6}$$

$$\boldsymbol{v} = \hat{\boldsymbol{z}}\times\nabla\phi = \left(-\frac{\partial\phi}{\partial y}, \frac{\partial\phi}{\partial x}\right), \tag{7}$$

$$\nabla^2\phi = n, \tag{8}$$

where $\hat{z}$ denotes the unit vector perpendicular to the plane and ∇ is the 2-d nabla.

It can be shown that the density field n is equal to the vorticity $\omega(\boldsymbol{r}) \equiv (\nabla\times\boldsymbol{v})_z$ of the 2-d velocity field $\boldsymbol{v}$ and the velocity field $\boldsymbol{v}$ is solenoidal ($\nabla\cdot\boldsymbol{v} = 0$), therefore, the set of equations (6)−(8) is equivalent to that of the Euler equation for the 2-d incompressible inviscid fluid with a free-slip (no-stress) boundary condition, but the vorticity

takes only a positive value in the present system.

To see the basic motion and the time scale, we consider the "pancake" state with the density field,

$$n(r) = \begin{cases} n_0 & (r \le R) \\ 0 & (r > R) \end{cases}, \tag{9}$$

which is a steady solution of eq. (6)−(8). The system shows a rigid rotation with the period

$$\tau_{\rm rot} \equiv \frac{r}{v_{\rm rot}(r)} = \frac{4\pi}{n_0}. \tag{10}$$

This period gives the approximate time scale for the macroscopic dynamics of the system of point vortices with the average density $n_0 \approx \pi N/R^2$.

If the system contains macroscopic numbers of electrons that follow eq. (2), and their distribution can be represented by a smooth density field $n_{\rm m}(x, y)$ obtained through averaging over a finite size mesh, i.e. coarse graining, then the density field should follow the following partial differential equations:

$$\frac{Dn_{\rm m}}{Dt} \equiv \frac{\partial n_{\rm m}}{\partial t} + \boldsymbol{v}_{\rm m} \cdot \nabla n_{\rm m} = C(n_{\rm m}), \tag{11}$$

$$\boldsymbol{v}_{\rm m} = \hat{\boldsymbol{z}} \times \nabla \phi_{\rm m} = \left(-\frac{\partial \phi_{\rm m}}{\partial y}, \frac{\partial \phi_{\rm m}}{\partial x} \right), \tag{12}$$

$$\nabla^2 \phi_{\rm m} = n_{\rm m}. \tag{13}$$

These are almost the same with eqs. (6) − (8), but there is the extra term $C(n_{\rm m})$ in the right hand side of eq. (11). This comes from the averaging on n and represents microscopic processes, thus it is called the collision term, since it is analogous to the corresponding term in the Boltzmann equation for the kinetic theory of gases. Note that, in experimental situations, we observe the particles density in a finite resolution, therefore the averaging operations are essential in macroscopic observations.

When the system contains macroscopic number of particles, the collision term is small, but it eventually causes the slow relaxation that leads the system to the equilibrium state, and estimating the effects of the collision term is still under intense discussion.

2.3 Constants of the dynamics

The Hamiltonian H is a constant of the dynamics, and is expressed in terms of the field variables as

$$\begin{aligned} H &= -\frac{1}{2} \int d^2\boldsymbol{r} \int d^2\boldsymbol{r}'\, n(\boldsymbol{r}) n(\boldsymbol{r}') G(\boldsymbol{r}, \boldsymbol{r}') \\ &= -\frac{1}{2} \int d^2\boldsymbol{r}\, n(\boldsymbol{r}) \phi(\boldsymbol{r}) \\ &= \int d^2\boldsymbol{r}\, \frac{1}{2} \boldsymbol{v}^2(\boldsymbol{r}), \end{aligned} \tag{14}$$

which corresponds to the total energy.

In the case of a system with circular symmetry, the total angular momentum I around the center of the system,

$$\begin{aligned} I &\equiv \sum_i^N r_i^2 \\ &= \int d^2\boldsymbol{r}\, r^2 n(\boldsymbol{r}) \\ &= \int d^2\boldsymbol{r}\, (\boldsymbol{r} \times \boldsymbol{v}(\boldsymbol{r}))_{\rm z}, \end{aligned} \tag{15}$$

is also a constant of the dynamics.

Since the 2-d Euler equation (6) − (8) represents an area-preserving dynamics, it has a set of conserved quantities, called Casimir constants,

$$Z \equiv \int d^2\boldsymbol{r}\, f(n(\boldsymbol{r})), \tag{16}$$

where $f(n)$ is an arbitrary function of the density field n. In the point vortex system, however, the Casimirs Z cannot be defined except for the linear combination of the total number of particles N

$$N \equiv \int d^2\boldsymbol{r}\, n(\boldsymbol{r}) \tag{17}$$

since the density field n has singularity of the delta function as in eq. (5).

2.4 Stability and evolution of states

In this subsection, we focus on the macroscopic behavior of the particle density $n(\boldsymbol{r})$ obtained from coarse-grained observation (From now on, we drop the subscript 'm' from the coarse-grained field, $n_{\rm m}(\boldsymbol{r})$ etc.).

It can be shown that the rotationally symmetric state with the density $n(r)$ being a decreasing function of r is not linearly unstable and is a numerically stable solution of eqs. (6) − (8). By contrast, the ring state, where the electrons are distributed in a ring-shaped region, is linearly unstable, and its instability is called diocotron instability.[33]

After the diocotron instability, nonlinear effects including the complex stretching and folding of the density structure take places. These deformation causes a fine filament-like structure, which will soon become too

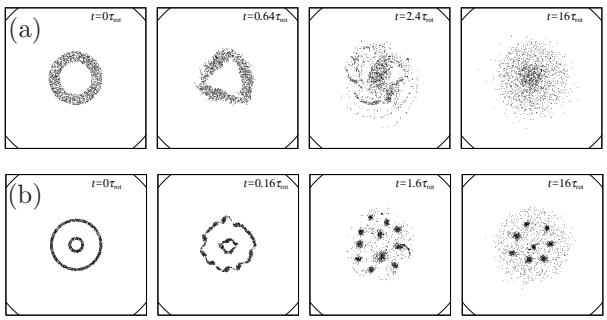

Fig. 2. Time evolution of electron density distributions from (a) a single ring initial state, and (b) a double ring initial state. Initial distributions are shown in the left-most figures and quasi stationary states are shown in the right-most figures. The conductor wall boundary is expressed by the solid arcs at the corner of the plotted area.

small to be observed in a finite resolution, and the system quickly approaches a quasi-stationary state.[15]

Figure 2 shows two examples of the time sequences, which start from the two unstable initial states and lead to two types of quasi-stationary states. Figure 2(a) shows the sequence that starts from a single-ring configuration, destabilizes into the mode three, and eventually falls into a singly peaked stable density distribution. In the case of Fig. 2(b), the instability of a double-ring initial configuration leads to a higher mode to break into many vortices, which merge occasionally while they undergo a collective chaotic motion, and eventually several surviving vortices form a regular structure, which does not undergo further change during our simulation time; such a state is called a vortex crystal state.[9]

These quasi-stationary states are in general not the equilibrium states;[15] the quasi-stationary states strongly depend on the initial states, which indicates that the system lacks the ergodicity in this time scale. For longer time scale, these quasi-stationary states relax into the equilibrium states, which we study in detail in the followings.

3. Statistical theories for diffusion and relaxation

In this section, we briefly review some of the elements of statistical theory for the slow relaxation.

3.1 Maximum one-body entropy distribution for equilibrium state

First, we describe the equilibrium state, which should be given by the state that maximizes the entropy under some constraints if the system is ergodic.

Within the one-body approximation,[4,6,7] the entropy and the energy are approximated by the one-body entropy S_1 and the mean field energy $H_{\rm MF}$ using the coarse-grained density $n(\boldsymbol{r})$ as,

$$S_1 = -\int d^2\boldsymbol{r}\, n(\boldsymbol{r}) \log n(\boldsymbol{r}). \tag{18}$$

$$H_{\rm MF} = -\frac{1}{2}\int d^2\boldsymbol{r} \int d^2\boldsymbol{r}'\, n(\boldsymbol{r}) G(\boldsymbol{r},\boldsymbol{r}') n(\boldsymbol{r}'), \tag{19}$$

where $n(\boldsymbol{r})$ is normalized to N as in eq. (17). The angular momentum I is evaluated by substituting the coarse-grained density $n(\boldsymbol{r})$ into eq. (15). Then the theory becomes simple and the maximum one-body entropy state is obtained[8] by maximizing eq. (18) with respect to $n(\boldsymbol{r})$ under the constraints of N, $H_{\rm MF}$ and I as

$$n(\boldsymbol{r}) = \exp(-1 - a + b\phi(\boldsymbol{r}) - cr^2). \tag{20}$$

with the Lagrange multipliers a, b, and c. From eq. (8), ϕ satisfies

$$\nabla^2\phi(\boldsymbol{r}) = \exp(-1 - a + b\phi(\boldsymbol{r}) - cr^2), \tag{21}$$

which can be solved numerically .

Note that S_1 would be a Casimir constant if the density field strictly followed the Euler equation (6).

3.2 Velocity distribution of randomly placed point vortex system

The velocity distribution of particles is an important element in the kinetic theory. In an ordinary system, the velocities and the positions of particles are two sets of dynamical variables that define a state. In the present system of the point vortices, however, the velocities are determined by the positions, and its distributions has been analyzed in terms of Levy's stable distribution.[34–37]

Let us consider the pancake density distribution, where the particles are located randomly with a constant average density within a radius R. The system undergoes a rigid bulk rotation with the period $\tau_{\rm rot}$ on average. At the center of the system, the particles have no average velocity and only the velocity fluctuation exists. For large N, the velocity distribution at the center of the system has been found to be the Gaussian with the variance proportional to $n \log N$ for the small velocity region, and the power-law V^{-4} in the large velocity region,[25]

$$W(\boldsymbol{V}) = \begin{cases} \frac{4}{n\gamma^2 \log N} \exp(-\frac{4\pi}{n\gamma^2 \log N} V^2), & (V \ll V_{\rm crit}(N)) \\ \frac{n\gamma^2}{4\pi^2 V^4}, & (V \gg V_{\rm crit}(N)), \end{cases} \tag{22}$$

with the crossover velocity

$$V_{\rm crit}(N) \sim \left(\frac{n\gamma^2}{4\pi}\log N\right)^{1/2} [\log(\log N)]^{1/2}, \tag{23}$$

where γ is the circulation (or electric charge) of a particle and normalized to unity in this paper. Note that the power law behavior of the distribution in large V comes from the distance distribution of the closest particles among the randomly located particles.

3.3 Kinetic theory of point vortex system

Exploiting the similarity to the relaxation process of the self-gravitating system,[20] Chavanis has developed the kinetic theory for the point vortex system.[24,25] As we have described, there are two relaxations, i.e. the fast relaxation and the slow relaxation; we will briefly review some of his results for the slow relaxation.

After the system establishes a quasi-stationary state following the Euler equation, small effects of the collision term in eq. (11) gradually stir the system to cause the slow relaxation, or the collisional relaxation. Chavanis has estimated the time scale of the collisional relaxation in terms of the diffusion of point vortices caused by the collision term as follows.

Assume that the velocity distribution is the Gaussian given in eq. (22) for the whole V region, then we can estimate the typical velocity $V_{\rm typ}$ from the mean square velocity as,

$$V_{\rm typ}^2 \equiv \langle V^2 \rangle = \frac{n\gamma^2}{4\pi}\log N. \tag{24}$$

For the pancake state with the flat distribution, there is no shear flow, thus the diffusion constant D may be estimated as

$$D \sim l_0 V_{\rm typ} \sim \gamma\sqrt{\log N} \tag{25}$$

where $l_0 \sim 1/\sqrt{n_0}$ is the average inter-particle distance.

For the state with singly peaked distribution, there

exists the shear flow around the peak, therefore, the diffusion is not isotropic. The diffusion coefficient for the radial direction may be estimated as

$$D \sim \tau V_{\rm typ}^2 \sim \frac{\gamma n(\boldsymbol{r})}{|\Sigma(\boldsymbol{r})|}\log N \tag{26}$$

where the correlation time τ has been estimated as $\tau \sim 1/|\Sigma|$ with the local shear

$$|\Sigma(\boldsymbol{r})| = r\frac{d}{dr}\left(\frac{V(r)}{r}\right). \tag{27}$$

If the slow relaxation is due to this diffusion process, the relaxation time $\tau_{\rm relax}$ would be the time for a particle to diffuse over the system size:

$$\tau_{\rm relax} \sim \frac{L^2}{D} \sim \frac{N}{\sqrt{\log N}}\tau_{\rm rot} \tag{28}$$

for the pancake state without shear flow, and

$$\tau_{\rm relax} \sim \frac{L^2}{D} \sim \frac{N}{\log N}\tau_{\rm rot} \tag{29}$$

for the singly peaked state with shear flow. In the both cases, $\tau_{\rm relax}$ increases almost linearly with N in units of the bulk rotation time.

4. Simulation method

We simulate the point vortex system by integrating eqs. (2) – (4).[38] Number of particles N ranges over $N = 128 \sim 2048$. Force acting on each particle is calculated by the simple sum of Coulomb force from all the other particles, therefore computational complexity of calculating the interactions is $O(N^2)$ for each time step. Numerical integration in time is performed using the second-order Runge-Kutta method. The time step of the integration is $\Delta t = 0.005\tau_{\rm rot}/4\pi$. The error ΔH in the total energy H tends to increase almost linearly in time, and the average increase of the error is $\Delta H/H \sim 10^{-5}$ for $N = 128$ and $\Delta H/H \sim 10^{-7}$ for $N = 2048$ per bulk rotation period $\tau_{\rm rot}$.

Initial configurations of particles are generated using random number sequences to be consistent with a given macroscopic density distribution. The problem is that, if two particles are too close to each other, they rotate around each other with large velocity; This could cause large integration error. To avoid this problem, we restrict the distance between any pair of particles to be larger than a certain limit length proportional to $\sqrt{\Delta t/N}$ in an initial configuration. This restriction is implemented by re-generating a particle position if the newly placed particle is too close to the existing particles. It should be noted, however, that such initial condition does not ensure that the particles do not come close to each other in future.

The unit length is defined so that the average square distance λ^2 from the center to be

$$\lambda^2 \equiv \frac{\sum_i^N r_i^2}{N} = \frac{1}{2}, \tag{30}$$

which is the angular momentum (15) per particle, hence, is a constant of dynamics. The radius of the container $R_{\rm w}$ is chosen as

$$R_{\rm w} = 2.9, \tag{31}$$

which is comparable to that in the experiments.[8,9] With this value, the container does not impose any conceivable restrictions on the relaxation process.

5. Simulation results

In this section we present our simulation results, mainly on the slow relaxation process in comparison with the kinetic theory by Chavanis.

After describing a couple of system setups used in the numerical simulation (§5.1), we present general behavior of the system and show that the time scale of the slow relaxation grows almost linearly with N (§5.2). The velocity distributions are shown in §5.3. Particle trajectories are examined in §5.4 to find anomalous diffusion, which is analyzed in terms of the Levy flight by decomposing the trajectories into sequences of steps, whose length and duration distributions are found to be of the power laws (§5.5).

5.1 Initial configurations

We will present simulation data mainly for the system setups that starts from two different initial states, which we call Setup A and Setup B in the following.

Setup A is the simulation that starts from the pancake state with a constant macroscopic density distribution in the region $r < R_0$, where the radius of the outer edge of the pancake R_0 is determined by the condition (30). In the continuum limit, this pancake state is the minimum energy state for a given angular momentum, therefore, the system cannot relax macroscopically.

Setup B is the simulation that starts from a double ring distribution. The particles are distributed in the regions $0.4R_0 < r < 0.6R_0$ and $0.8R_0 < r < R_0$. In this case, the system relaxes into a singly peaked state with shear flow, as we will see below.

The numbers of particles N are same for both setups A and B. The relaxation properties of the macroscopic density are mainly obtained from Setup B of the double ring initial state. Setup A of the pancake initial state is used to investigate the diffusion process of individual point vortices.

Another variation of initial configuration, which we call Setup B', is used in Fig. 6 in order to see the initial state dependence of the slow relaxation. Setup B' is the simulation that starts from a single ring distribution. The particles are distributed in the regions $0.4R_0 < r < R_0$. The energy happens to be almost the same with that of Setup B. The system relaxes into a singly peaked state.

5.2 Fast and slow relaxation

Figure 4 shows the time development of the one-body entropy $S_1(t)$ as a function of time t in the semilogarithmic scale. The one-body entropy is calculated by coarse-graining the distribution of point vortices using a mesh shown in Fig. 3. The size of the cell at distance r from the center is $\delta r = R_{\rm w}/m_r$ in the radial direction and is $r\delta\theta = 2\pi R_{\rm w}/m_r$ in the azimuthal direction, where m_r is the number of division in the radial direction, thus the

shape of a cell is elongated in the azimuthal direction. This gives the area of a cell $\delta A \approx (\delta r)(r\delta\theta) = 2A/m_r^2$ where $A = \pi R_{\rm w}^2$ is the total area of the system. Here, $m_r = 20$ is used for all the simulations.

We observe three stages in the development of $S_1(t)$: (i) diocotron instability ($t \lesssim 1\tau_{\rm rot}$), where $S_1(t)$ is almost constant, (ii) fast relaxation ($1\tau_{\rm rot} \lesssim t \lesssim 10\tau_{\rm rot}$), where $S_1(t)$ shows a rapid increase, and (iii) slow relaxation ($10\tau_{\rm rot} \lesssim t$), where $S_1(t)$ increases slowly with time.

The one-body entropy $S_1(t)$ as a function of time t in the fast relaxation is shown in Fig. 5 for various N. We do not observe the systematic N-dependence of the relaxation time scale if we scale the time t by the bulk rotation period $\tau_{\rm rot} \propto 1/N$.

Figure 6 shows the time evolutions of the density distributions as a function of r. The initial states are the double ring initial state (Setup B) (a), and the single ring initial state (Setup B') (b). The maximum one-body entropy state is also shown by the thick solid lines for comparison. The energy and the angular momentum are same for these two cases, so that the maximum one-body entropy state is same for the both cases. Although the quasi-stationary state achieved after the fast relaxation depends on the initial state, after the slow relaxation, the density distribution approaches the maximum one-body entropy state in both cases. Another example is shown in Fig. 7, where the initial single ring state relaxes into the vortex crystal state after the fast relaxation, but the vortices are smeared to merge into a single broad peak and the state eventually approaches the maximum one-body entropy state through the slow relaxation.

Figure 8 shows that the time development of the one-

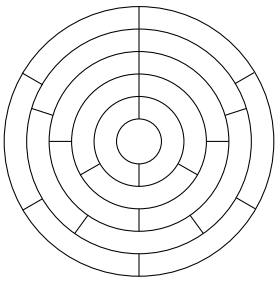

Fig. 3. An example of mesh used to observe the macroscopic density field for one-body entropy calculation. Number of partition in azimuthal direction increases by one as r increases (in the figure, $1, 2$ and 3 from the center to the periphery). In the actual observations, the resolution in radial direction m_r is $m_r = 20$.

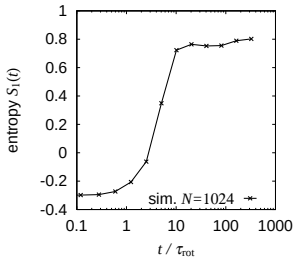

Fig. 4. Time development of the one-body entropy $S_1(t)$ in the semilogarithmic scale for Setup B with $N = 1024$.

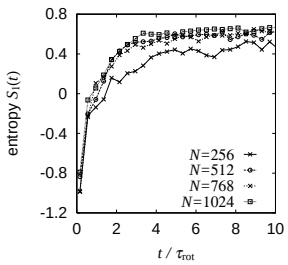

Fig. 5. Time evolution of the one-body entropy S_1 during the fast relaxation for various N for Setup B. The time t is scaled by the bulk rotation time $\tau_{\rm rot} \propto 1/N$.

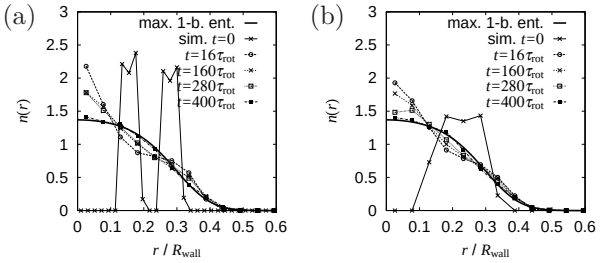

Fig. 6. Time development of the density distribution vs. r for the double ring initial state (Setup B) (a), and the single ring initial state (Setup B') (b). In the both cases, the number of particles is $N = 1024$ and the energy are almost the same for the both cases. The maximum one-body entropy state is also shown by the thick solid curves. For each curves of simulation results, the density distribution is averaged over 100 samplings at different times within the duration of about 10 rotations.

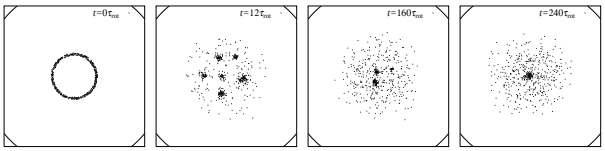

Fig. 7. Time evolution of the point vortex distribution with $N = 512$. The initial state is the single ring state with a constant density at $0.9R_0 < r < R_0$ of randomly placed particles.

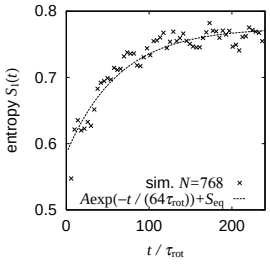

Fig. 8. Time evolution of the one-body entropy S_1 during the slow relaxation for Setup B with $N = 768$. The simulation data are averaged over 100 successive points. The dashed curve shows an exponential decay of eq. (32), with the fitting parameters $S_{\rm eq} = 0.775$, $A = 0.19$, and $\tau_{\rm relax} = 64\tau_{\rm rot}$.

body entropy $S_1(t)$ during the slow relaxation can be approximated by the exponential form:

$$S(t) \approx S_{\rm eq} - A\exp(-t/\tau_{\rm relax}). \tag{32}$$

We determine the parameters $S_{\rm eq}$, A and $\tau_{\rm relax}$ by fitting with the simulation data. The relaxation time scale $\tau_{\rm relax}$ is plotted against the number of particles N in Fig. 9. We find that $\tau_{\rm relax}$ increases almost linearly with N if $\tau_{\rm relax}$ is measured in the unit of the bulk rotation time $\tau_{\rm rot} \propto 1/N$. This is consistent with the theory of Chavanis in §3.3.

5.3 Velocity distribution

Figure 10 shows the radial velocity distributions of the simulations of Setup A (the pancake state) (a), and Setup B (the singly peaked state)(b). In both cases, we measure the velocity distribution in the same time region $80\tau_{\rm rot} \le t \le 240\tau_{\rm rot}$, which is within the slow relaxation for the case of the singly peaked state (b), while the pancake state (a) does not show any macroscopic relaxation. Only the distributions of the radial component of velocity are plotted because the azimuthal velocity contains the average bulk rotation.

In Fig. 10(a), the Gaussian distribution that scales as $v/(N\log N)$ is observed for small v, as is expected by the theory in §3.3.[25,34–36] For large v, however, we find the exponential tail instead of the power law tail.

The reason of the lack of the power law tail seems to be the restriction of the particle distance imposed on the initial state, as is explained in §4. If we remove this restriction and locate the particles randomly, then we obtain the tail closer to the power law v^{-4}, as shown in Fig. 11. Note that the precision of the energy conservation is poor for the simulation without the restriction.

For the singly peaked state (Fig. 10(b)), we find that the distribution is broader than that for the pancake case (a) but the tail is still exponential. Although the distribution does not fit to the Gaussian very well, it is still scaled by $v/(N\log N)$ in small v region.

5.4 Anomalous diffusion

Figure 12 shows a trajectory of the radial position of a particle in the quasi-stationary state. One can see that the motion of a particle looks like a random walk, while it occasionally undergoes long jumps with a step almost of the system size ($\Delta r \sim 1$).

To see the diffusion behavior, the time development of the mean square radial deviation $\langle(\Delta r(t))^2\rangle$ where $\Delta r(t) = r(t) - r(0)$ is plotted in Fig. 13(a) for the pancake case with various N (Setup A). We observe a superdiffusion

$$\langle(\Delta r(t))^2\rangle \sim t^{\gamma}, \tag{33}$$

with the diffusion exponent $\gamma = 1.75 \pm 0.1 > 1$ for all N. The square radial deviation saturates in $\langle(\Delta r(t))^2\rangle \approx 0.1$ due to the finite system size $L \sim 1$. From Fig. 13(b), we obtain $\gamma = 1.85 \pm 0.1$ for the case of Setup B (the singly peaked state).

Figure 14 shows the "coefficient of anomalous diffu-

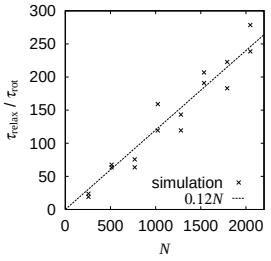

Fig. 9. Relaxation time $\tau_{\rm relax}$ of the one body entropy in the slow relaxation as a function of the number of particles N. The y-axis is normalized by the bulk rotation time $\tau_{\rm rot}$. The simulation is by Setup B.

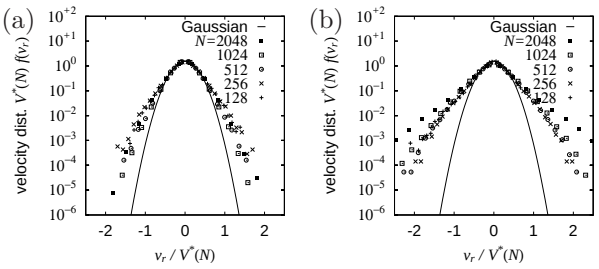

Fig. 10. Distributions of the radial component of velocity of two different simulation setups: Setup A (the pancake state) (a), and Setup B (singly peaked state) (b). The velocity is scaled by $V^*(N) \equiv N\log N$. The distribution functions are averaged over 200 samplings at different times during the slow relaxation, $80\tau_{\rm rot} \le t \le 240\tau_{\rm rot}$.

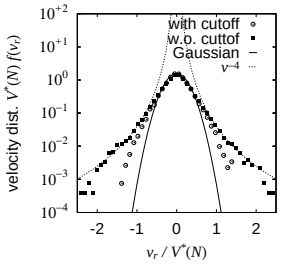

Fig. 11. Distributions of the radial component of velocity for Setup A with (◯) and without (■) the restriction on the distance between the particles (see §4). The number of particles is $N = 128$. The velocity is scaled by $V^*(N) \equiv N\log N$. The distribution functions are averaged over 200 samplings at different times during the slow relaxation, $80\tau_{\rm rot} \le t \le 240\tau_{\rm rot}$.

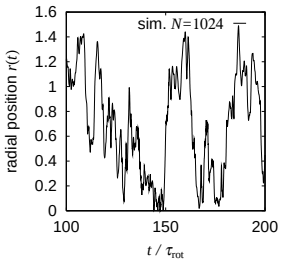

Fig. 12. Time development of the radial position of a particle for Setup B (the singly peaked state) with $N = 1024$.

sion" defined as

$$D_N = \frac{\langle (\Delta r(t))^2 \rangle}{t^\gamma}, \tag{34}$$

as a function of N. We find a power law dependence on N as $D_N \sim N^\eta$ with $\eta = 0.85 \pm 0.1$.

Figure 15 shows the distribution function $P(\Delta r|t)$ of the deviation Δr at various times t. The data are taken from the same simulation with that in Fig. 13 (a) for $N = 2048$. We see that the distribution curves overlap by the scaling, $\Delta r/t^{\gamma/2}$ with $\gamma = 1.75$. which shows the width of the distribution grows as $t^{\gamma/2}$. The tail of the distribution converges to zero faster than the exponential.

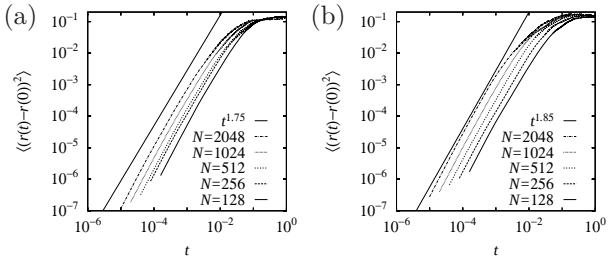

Fig. 13. Time evolution of the mean square of the difference of radial position $\Delta r(t) = r(t) - r(0)$ from its initial position in the log-log plot. The simulation setups are Setup A (the pancake state) (a), and Setup B (the singly peaked state) (b).

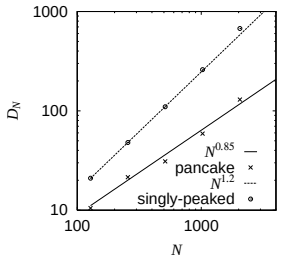

Fig. 14. Coefficient of anomalous diffusion $D_N = \langle \Delta r^2 \rangle / t^\gamma$ as a function of the number of particles N. The coefficient D_N are estimated from the plots in Fig. 13. $\gamma = 1.75$ is used for Setup A (the pancake state), and $\gamma = 1.85$ is used for Setup B (the singly peaked state).

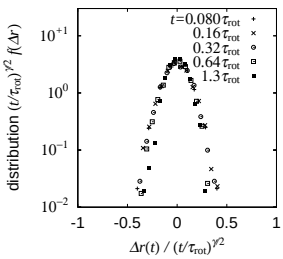

Fig. 15. Distribution $P(\Delta r|t)$ of the deviation of the radial position $\Delta r(t) = r(t) - r(0)$ at various times t. The plotted data are same with those in Fig. 13(a) for $N = 2048$. The deviation Δr is scaled by $t^{\gamma/2}$ with the same exponent $\gamma = 1.75$ with Fig. 13(a).

5.5 *Random walk and Levy flight*

In order to analyze the above diffusive trajectories as shown in Fig. 12, we decompose them into "steps". Each step is defined as the interval between two successive extrema in the radial motion $\Delta r(t)$, thus each step has a step length l and a step time τ. Then the radial position Δr and the elapsed time t at M-th step are expressed by

$$\Delta r = \sum_{k=1}^{M} l_k, \quad t = \sum_{k=1}^{M} \tau_k. \tag{35}$$

Figure 16(a) shows the distributions of the step length in the simulations of Setup A (the pancake state) with various N, which exhibits the power law decay in the large step length. The step length distributions for various N seem to overlap with each other if we scale the step length as $l\sqrt{N}$, which indicates that the lower cutoff of the power law scales as $l_{\min} \sim 1/\sqrt{N}$. The upper cutoff of the power law decay is given by the system size, thus it does not depend on N. The power law distribution is expressed in the form of $p(l) \sim l^{-(1+\mu)}$ and the exponent $\mu = 0.7 \pm 0.1$ is obtained. We find that the distribution function is almost symmetric both for the positive l (jump towards the periphery) and the negative l(jump towards the center).

Figure 16(b) shows the similar distribution function obtained for the step time τ, which is normalized by the bulk rotation time $\tau_{\rm rot} \propto 1/N$. The power law exponent χ is defined by $p(\tau) \sim \tau^{-(1+\chi)}$ and $\chi = 0.55 \pm 0.1$ is obtained. The lower cutoff of the power law scales as $\tau_{\min} \sim 1/N$.

Figure 17 shows the step length distribution $p(l)$ and the step time distribution $p(\tau)$ for the singly peaked state (Setup B).

Table I summarizes the exponents obtained in our simulations; μ's and χ's are the power law exponents of the step size distributions $p(l)$ and $p(\tau)$, respectively, and their values are obtained from Figs. 16 and 17. The exponents of the anomalous diffusion γ from the simulation results in Fig. 13, and the exponents η for the N dependence of the anomalous diffusion coefficient $D_N \sim N^\eta$ from Fig. 14 are also listed. The exponents $\gamma_{\rm est}$ and $\eta_{\rm est}$

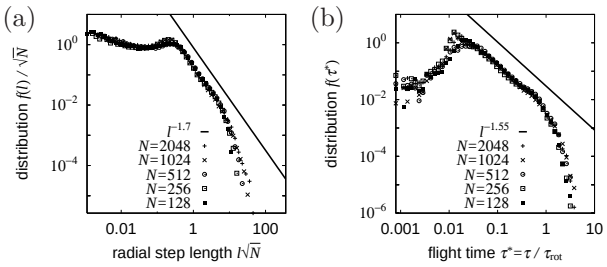

Fig. 16. Distribution functions for the step length l for the radial direction scaled by $\sqrt{N}$ (a), and step time $\tau^* = \tau/\tau_{\rm rot}$ in units of the bulk rotation time $\tau_{\rm rot}$ (b). The simulation is by Setup A (the pancake state). The step length l is defined as a distance between two neighboring turns in the trajectories of the radial position of a particle, and τ is duration time needed for a step. For each simulation with N, 64 particles are randomly chosen and their trajectories are analyzed in the slow relaxation, $80\tau_{\rm rot} \le t \le 240\tau_{\rm rot}$.

are the exponents derived from the step distribution exponents (see §6).

Now we examine the correlation in the step sequences. Let the step length and step time of the k-th step be l_k and τ_k, respectively. The correlations $\langle l_0 l_k \rangle$ and $\langle \tau_0 \tau_k \rangle$ are plotted against k for the pancake state (Setup A) in Fig. 18. These correlations show the exponential decay, which indicates that the correlation in the step sequences is short-range.

In order to analyze the step sequence in more detail, we define $P(|\Delta r| \,|M)$ and $P(t|M)$ as the distributions of the distance Δr and the time t at the M-th step (eq. (35)), respectively. Contour plots of these distribution functions are shown in Fig. 19. The value of the distributions are shown in the proportion to the peak value $p_{\rm peak}(M)$ of

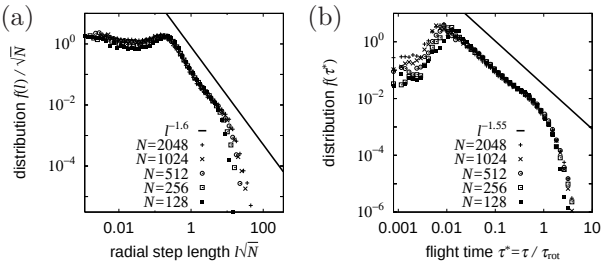

Fig. 17. Distribution functions for the step length l for the radial direction scaled by $\sqrt{N}$ (a), and the step time $\tau^* = \tau/\tau_{\rm rot}$ in the unit of the bulk rotation time $\tau_{\rm rot}$ (b). The simulation is by Setup B (the singly peaked state). The data are collected in the same way as in Fig. 16

Table I. Exponents for the step time distributions χ, the step size distributions μ, and the anomalous diffusion exponents γ and η and the derived exponents $\gamma_{\rm est} = 2\chi/\mu$ and $\eta_{\rm est} = 2\chi/\mu - 1$ from χ and μ See texts for the definition of each exponent.

Setup	χ	μ	γ	η
A	0.55 ± 0.1	0.7 ± 0.1	1.75 ± 0.1	0.85 ± 0.1
B	0.55 ± 0.1	0.6 ± 0.1	1.85 ± 0.1	1.2 ± 0.1
Setup			$\gamma_{\rm est}$	$\eta_{\rm est}$
A			1.6	0.6
B			1.8	0.8

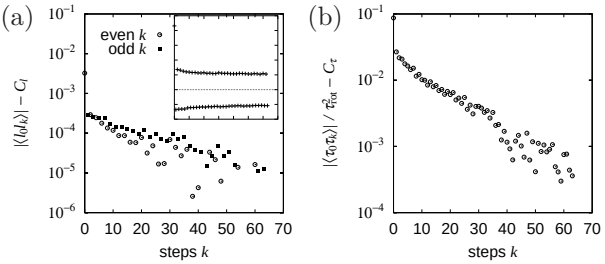

Fig. 18. Correlation functions in the step sequences of the step length $\langle l_0 l_k \rangle$ (a), and the step time $\langle \tau_0 \tau_k \rangle$ (b) as a function of k. The simulation is by Setup A (the pancake state) with $N = 2048$. These data are obtained from trajectories of randomly chosen 64 particles in the slow relaxation process, $80\tau_{\rm rot} \le t \le 240\tau_{\rm rot}$. The fitting parameters are $C_l = 0.00107$ and $C_\tau = 0.539$. The inset in (a) shows a linear plot of step correlation in the same range of k.

$P(|\Delta r| \,|M)$ or $P(t|M)$ for each step M so that one can compare the width of the distributions between different M's. We observe that the width of $P(|\Delta r| \,|M)$ and the peak position of $P(t|M)$ increase by the powers of M, as

$$(\Delta r)^2 \sim M^{2/\mu^*}, \quad t \sim M^{1/\chi^*} \tag{36}$$

with $\mu^* = 1.1 \pm 0.2$ and $\chi^* = 0.85 \pm 0.1$.

Note that the contour curves are almost equally spaced in the logarithmic scale, which means that the distribution functions have the power-law tail. The growth of the tail of the distribution function $P(|\Delta r| \,|M)$ is saturated for large M where the tail approaches $\Delta r \sim 1$, or the system size.

6. Analyses

As we have shown in §5.5, the step length distribution $p(l)$ and the step time distribution $p(\tau)$ have the power law tail, and the correlation between the steps decays exponentially. Based on these observations, we analyze the diffusion process in terms of the Levy flight and derive the exponents. Some of the basic properties of the Levy flight are summarized in Appendix.

The typical radial deviation of position Δr_M and the typical elapsed time t_M after the M-th step can be estimated by Levi flight as

$$\Delta r_M^2 \sim M^{2/\mu} l_{\rm min}^2, \quad t_M \sim M^{1/\chi} \tau_{\rm min}, \tag{37}$$

from eq. (A·8).

These should be compared with eq. (36), which are direct observation of $P(\Delta r|M)$ and $P(t|M)$. Both of them show the power law of M, but the values of the exponents μ^* and χ^* estimated from the direct observation are not very close to the values of μ and χ from the step distribution. we suspect this discrepancy is due to the finite size effect as we have mentioned at the end of §5.5.

Keeping this limitation in mind, let us continue the analysis based on the Levy flight picture; The expression (37) show that the total sums of eq. (35) are of the same order of the largest step out of the M steps. This means that most of the contribution to eq. (35) comes from the largest step. We assume this largest step to be the same

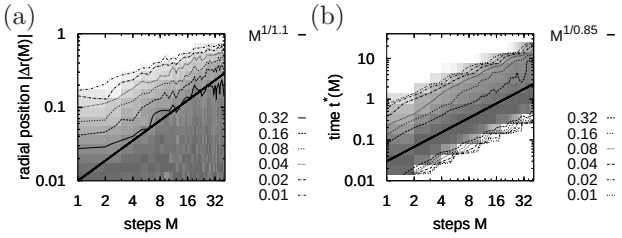

Fig. 19. Contour plots for the distribution of radial position $P(|\Delta r| \,|M)$ (a), and that of the time $P(t^*|M)$ (b) as a function of the number of steps M in the logarithmic scale. $t^* = t/\tau_{\rm rot}$ and the distribution functions are normalized by the peak distribution $p_{\rm peak}(M)$ for each step M. The thick lines are $|\Delta r| \propto M^{1/\mu^*}$ (a) and $t^* \propto M^{1/\chi^*}$ (b) with $\mu^* = 1.1$ and $\chi^* = 0.85$ that are obtained by fitting. The data are obtained from trajectories of randomly chosen 64 particles in the time duration, $80\tau_{\rm rot} \le t \le 240\tau_{\rm rot}$. For both figures, the simulation is by Setup A (the pancake state) with $N = 2048$.

step for Δr and t. This is natural assumption because shorter steps are results of waggling motion caused by nearly vortices, vortices tend to move faster during the shorter steps.

Using the assumption, the typical radial position Δr_t at time t can be estimated by simply eliminating M in eq. (37). Identifying t_M as t, we have

$$\Delta r_t^2 \sim D_N t^{2\chi/\mu} \tag{38}$$

with

$$D_N \sim \frac{l_{\min}^2}{\tau_{\min}^{2\chi/\mu}}. \tag{39}$$

Comparing eq. (38) with eq. (33), we see that the anomalous diffusion exponent γ is related with χ and μ as

$$\gamma = 2\chi/\mu. \tag{40}$$

The dependence of the anomalous diffusion coefficient D_N on the number of particles N is also obtained from eq. (39). Assuming that the short length cutoff of the step length distribution $l_{\min}$ is approximately given by the average particle distance l_0, thus we have

$$l_{\min}^2 \approx l_0^2 \sim n_0^{-1} = \frac{\pi L^2}{N} \tag{41}$$

Similarly, we assume that the short time cutoff of the step time distribution $\tau_{\min}$ is given by the rotation time of the vortex pair τ_0 with the distance l_0:

$$\tau_{\min} \approx \tau_0 \sim \frac{l_0}{v_0} \sim N^{-1} \tag{42}$$

where v_0 is the rotation velocity of the paired vortices with the distance l_0, and given by

$$v_0 \sim \frac{q}{l_0}, \tag{43}$$

from the 2-d Coulomb law. Here, q is the charge of a particle, which is normalized to unity. Note that these N dependences are consistent with the scaling form of the step size distributions $p(l)$ and $p(\tau)$ in Figs. 16 and 17. Substituting these cutoffs into eq. (39), we obtain N dependence of the coefficient D_N,

$$D_N \sim N^{2\chi/\mu-1}, \tag{44}$$

thus the exponent η as

$$\eta = 2\chi/\mu - 1 = \gamma - 1. \tag{45}$$

From the simulation results and the definition of the exponents, we obtain $\chi = 0.55$ and $\mu = 0.7$ for the radial direction in the pancake state (Setup A). Thus, from eqs. (40) and (44), one obtains $\gamma \approx 1.6$ and $\eta \approx 0.6$. Similarly, we obtain the exponents for the singly peaked state (Setup B). They are listed in Table I.

7. Summary and discussion

We have performed the numerical simulations on the two-dimensional point vortex model with a unit circulation of the same sign, in order to study the relaxation process of pure electron plasma under the strong magnetic field. Due to the long-range interaction between the vortices, the system behaves very differently from ordinary systems with short-range interaction.

We have found the following: (i) There exist two types of relaxation: the fast relaxation and the slow relaxation. The fast relaxation takes place with the time scale comparable with the bulk rotation time $\tau_{\rm rot}$ and leads the system to a quasi-stationary state following the Euler equation, while the slow relaxation takes place after the fast relaxation with the relaxation time $\tau_{\rm relax} \sim N\tau_{\rm rot}$ due to the individual motion of vortices; This is consistent with Chavanis' theory except for the $\log N$ correction. After the slow relaxation, the system reaches the maximum one-body entropy state. (ii) Individual motion of point vortices in the slow relaxation process is superdiffusive with the exponent $\gamma \approx 1.75$ for the pancake (shear free) state and $\gamma \approx 1.85$ for the singly peaked (with shear) state. The coefficient of anomalous diffusion depends on the number of particles N in the power laws. (iii) The superdiffusive motion of individual vortices can be decomposed into a sequence of steps. The correlations of the step length and that of the step time along the sequence are short range, and the distributions of the step length and the step time are of the power laws with the exponents μ and χ, respectively. The superdiffusive motion can be reconstructed from the Levy flight, i.e. the exponent γ for the anomalous diffusion and the exponent η for the N dependence of its coefficient are expressed as $\gamma = 2\chi/\mu$ and $\eta = 2\chi/\mu - 1$; the former expression agrees with the exponent from the simulation within the error bars, but the agreement of the latter is not good.

Among these results, our result (i) of the N dependence of the slow relaxation time seems to agree with Chavanis' estimation. However, his picture that the relaxation is due to the normal diffusion of the point vortices is not confirmed by our simulation results, but we observe the superdiffusive behavior in the simulations. If we estimate the relaxation time $\tau_{\rm relax}^*$ with anomalous diffusion by the similar way as he did for normal diffusion, then

$$\tau_{\rm relax}^* \sim \left(\frac{L^2}{D_N}\right)^{1/\gamma} \sim N^{1-\eta/\gamma}\tau_{\rm rot} \ll \tau_{\rm relax} \sim N\tau_{\rm rot}, \tag{46}$$

which gives much shorter relaxation time than that observed. This implies that the motions of point vortices are not independent of each other and provide only weak mixing. Actually we observe in our simulations that a point vortex tends to avoid "collisions" during the long jumps.

In the literature,[26,27] it has been pointed out that a test particle is convected for a long way comparable to the system size due to the existence of long-living large vortices. The diffusion coefficient proposed by Taylor and McNamara depends on time and converges to a constant only when $(\Delta r/L)^2 \gg 1$ holds, which suggests anomalous diffusion. Although these results are for the neutral plasma, its behavior of the anomalous diffusion seems consistent qualitatively with our simulation results on the non-neutral plasma.

Recently, Dubin and Jin performed fairly large-scale simulations on the 2-d point vortex system with a positive charge,[39,40] and determined the diffusion coefficients in the states without mean shear. Their results of the

diffusion coefficient show the $N^{1/2}$ dependence, which is consistent with that expected by Taylor and McNamara in the converging limit, but their values of diffusion constant from the simulations seem substantially smaller than those predicted by the theory: This may be due to the slow convergence mentioned in the above paragraph. They have also shown that the diffusion in the radial direction is normal under the external shear.

In experiments, the number of electrons is very large while the charge of each electron is very small. In the present model, the situation may correspond to the case in the limit of the infinite N with a fixed total charge, namely, a fixed bulk rotation time $\tau_{\rm rot}$, in which limit the slow relaxation never takes place and we only observe the quasi-stationary states. If this is the case, actual slow relaxation that may be observed in experiments should be due to non-ideal effects such as three dimensionality of the Malmberg trap, scattering at the end of the cylinder, impurities, etc.

Acknowledgments

The authors would like to thank Professor Y. Kiwamoto, Professor M. Sakagami, Dr. M. M. Sano, Dr. Y. Yatsuyanagi, T. Yoshida and Dr. D. Watanabe for valuable discussions and comments. They would also like to thank Professor P. H. Chavanis for his communication.

Appendix: Levy flight and anomalous diffusion

In this appendix, we summarize some basic formulas of the Levy flight.

Consider a random walk problem where the size of each step l is a random variable without correlation, then after the M-th step the particle position X is

$$X = \sum_i^M l_i. \tag{A·1}$$

If the distribution $p(l)$ of step size l has a finite second moment $\langle l^2 \rangle$, the central limit theorem tells us that the distribution of X at the M-th step is known to be the Gaussian distribution for large M and the dispersion increases as

$$\langle (X - \langle X \rangle)^2 \rangle \sim DM, \tag{A·2}$$

where D is the diffusion coefficient. This represents the normal diffusion law.

If the distribution function $p(l)$ is the power law with the diverging second moment,

$$p(l) \sim |l|^{-(1+\mu)}, \quad (0 < \mu < 2) \tag{A·3}$$

for large $|l|$, then the asymptotic form of the distribution of X at large M is given by the Levy's stable distribution.[41,42]

$$P(X|M) \to \begin{cases} \frac{1}{M^{1/\mu}} L_{\mu,\beta}\left(\frac{X}{M^{1/\mu}}\right), & (0 < \mu < 1), \\ \frac{1}{M^{1/\mu}} L_{\mu,\beta}\left(\frac{X - \langle X \rangle}{M^{1/\mu}}\right), & (1 < \mu < 2), \end{cases} \tag{A·4}$$

where $L_{\mu,\beta}(x)$ is the scaling form of the distribution of X at $M \to \infty$. The parameter β characterizes the degree of asymmetry, and is determined from the asymmetry of $p(l)$ for large $|l|$. The $\beta = 0$ case represents the symmetric distribution:

$$L_{\mu,0}(Z) \equiv \frac{1}{2\pi} \int_{-\infty}^{+\infty} dk \exp(ikZ - C|k|^\mu), \tag{A·5}$$

where C is a scaling factor. This gives the Gaussian distribution when $\mu = 2$. As for the $\beta = 1$ case, the distribution is given by

$$L_{\mu,1}(Z) \equiv \frac{1}{2\pi i} \int_{d-i\infty}^{d+i\infty} ds \exp(sZ - C's^\mu), \tag{A·6}$$

which is zero for $Z < 0$ representing a completely asymmetric case. The distribution $L_{\mu,\beta}(Z)$ has an approximate form of $L_{\mu,\beta}(Z) \sim Z^{-(1+\mu)}$ for large Z.

The fact that the above distribution function $P(X|M)$ scales as $X/M^{1/\mu}$ can be understood[41] by introducing the effective cutoff $l_{\rm c}$, to the step length distribution $p(l)$. By simple argument, one can see the cutoff depends on the number of steps M as

$$l_{\rm c} \sim M^{1/\mu} l_{\rm min}, \quad (0 < \mu < 1). \tag{A·7}$$

Then, a typical walk may be estimated as

$$X_M = \sum_i^M l_i \approx M\langle l \rangle \approx \int_{l_{\rm min}}^{l_{\rm c}} dl\, l\, p(l) \sim M^{1/\mu} l_{\rm min}, \quad (0 < \mu < 1), \tag{A·8}$$

which means the distribution function scales as $X/M^{1/\mu}$. Therefore, peak position $X_{\rm p} \sim M^{1/\mu}$ and the square of typical width $X_{\rm w}^2 \sim M^{2/\mu}$ of the distribution $P(X|M)$ at the M-th step can be considered as measures of the anomalous diffusion by the Levy flight, even though the distribution function has diverging moments.

1) P. Tabeling: Phys. Rep. **362** (2002) 1.
2) L. Onsager: Nuovo Cimento (Suppl.) **6** (1949) 279.
3) G. L. Eyink and K. R. Sreenivasan: Rev. Mod. Phys. **78** (2006) 87.
4) G. Joyce and D. Montgomery: J. Plasma Phys. **10** (1973) 107.
5) D. Montgomery and G. Joyce: Phys. Fluids **17** (1974) 1139.
6) P. A. Smith and T. M. O'Neil: Phys. Fluids **B2** (1990) 2961.
7) S. Kida: J. Phys. Soc. Jpn. **39** (1975) 1395.
8) X.-P. Huang and C. F. Driscoll: Phys. Rev. Lett. **72** (1994) 2187.
9) K. S. Fine, A. C. Cass, W. G. Flynn, and C. F. Driscoll: Phys. Rev. Lett. **75** (1995) 3277.
10) R. Robert and J. Sommeria: Phys. Rev. Lett. **69** (1992) 2776.
11) J. Sommeria, C. Staquet, and R. Robert: J. Fluid Mech. **233** (1991) 661.
12) J. Miller, P. B. Weichman, and M. C. Cross: Phys. Rev. A **45** (1992) 2328.
13) B. M. Boghosian: Phys. Rev. E **53** (1996) 4754.
14) D. Z. Jin and D. H. E. Dubin: Phys. Rev. Lett. **80** (1998) 4434.
15) R. Kawahara and H. Nakanishi: J. Phys. Soc. Jpn. **75** (2006) 054001.
16) H. Brands, P. H. Chavanis, R. Pasmanter, and J. Sommeria: Phys. Fluids **11** (1999) 3465.
17) P. Chen and M. C. Cross: Phys. Rev. Lett. **77** (1996) 4174.
18) V. Pavlov, D. Buisine, and S. Decossin: Phys. Fluids **14** (2002) 3937.
19) D. Lynden-Bell: Mon. Not. R. Astron. Soc. **136** (1967) 101.
20) T. Padmanabhan: Phys. Rep. **188** (1990) 285.
21) S. Chandrasekhar: Rev. Mod. Phys. **21** (1949) 383.
22) A. Taruya and M. Sakagami: Phys. Rev. Lett. **90** (2003) 181101.
23) M. Sakagami and A. Taruya: Continuum Mech. Thermodyn. **16** (2004) 279.

24) P. H. Chavanis: Phys. Rev. E **64** (2001) 026309.
25) P. H. Chavanis: in *Dynamics and Thermodynamics of Systems with Long Range Interactions, (Lecture Notes in Physics)*, ed. T. Dauxois, S. Ruffo, E. Arimondo, and M. Wilkens (Springer, Berlin, Heidelberg, 2002), pp. 208 – 289.
26) J. B. Taylor and B. McNamara: Phys. Fluids **14** (1971) 1492.
27) J. M. Dawson, H. Okuda, and R. N. Carlile: Phys. Rev. Lett. **27** (1971) 491.
28) O. Cardoso and P. Tableling: Europhys. Lett. **7** (1988) 225.
29) W. Young, A. Pumir, and Y. Pomeau: Phys. Fluids A **1** (1989) 462.
30) T. H. Solomon, E. R. Weeks, and H. L. Swinney: Phys. Rev. Lett. **71** (1993) 3975.
31) T. Yoshida and M. Sano: J. Phys. Soc. Jpn. **74** (2004) 587.
32) Y. Yatsuyanagi, Y. Kiwamoto, H. Tomita, M. M. Sano, T. Yoshida, and T. Ebisuzaki: Phys. Rev. Lett. **94** (2005) 054502.
33) R. C. Davidson: *Theory of Nonneutral Plasmas* (W. A. Benjamin, Inc., Reading, Mass., Tokyo, 1987).
34) H. Takayasu: Prog. Theor. Phys. **72** (1984) 471.
35) I. A. Min, I. Mezic, and A. Leonard: Phys. Fluids **8** (1996) 1169.
36) B. N. Kuvishinov and T. J. Schep: Phys. Rev. Lett. **84** (2000) 650.
37) This method has been originally developed by J. Holtsmark [Annalen der Physik. **58** (1919) 577.] for the force distribution of stellar system. For review, S. Chandrasekhar: Rev. Mod. Phys. **15** (1943) 1.
38) A. Leonard: J. Comput. Phys. **37** (1980) 289.
39) D. H. E. Dubin and D. Z. Jin: Phys. Lett. A **284** (2001) 112.
40) D. H. E. Dubin: Phys. Plasma **10** (2003) 1338.
41) J. P. Bouchaud and A. Georges: Phys. Rep. **195** (1990) 127.
42) B. V. Gnedenko and A. N. Kolmogorov: *Limit distributions for sums of independent random variables* (Addison-Wesley Publishing Company, Inc., Cambridge 42, Mass., 1954).